Optics Letters

Frequency-modulated microwave signal generation by dual-wavelength-injection period-one laser dynamics

Xiaoyue Yu, Guanqun Sun, Fangzheng Zhang,* and Shilong Pan

Key Laboratory of Radar Imaging and Microwave Photonics, Ministry of Education, Nanjing University of Aeronautics and Astronautics, Nanjing 210016, China
**Corresponding author: zhangfangzheng@nuaa.edu.cn*

Received 28 September 2022; revised 22 October 2022; accepted 23 October 2022; posted 26 October 2022; published 8 November 2022

In this Letter, dual-wavelength-injection period-one (P1) laser dynamics is proposed for the first time, to the best of our knowledge, to generate frequency-modulated microwave signals. By injecting light with two different wavelengths into a slave laser to excite P1 dynamics, the P1 oscillation frequency can be modulated without external control of the optical injection strength. The system is compact and stable. The frequency and bandwidth of the generated microwave signals can be easily adjusted by tuning the injection parameters. Through both simulations and experiments, the properties of the proposed dual-wavelength injection P1 oscillation are revealed, and the feasibility of the frequency-modulated microwave signal generation is verified. We believe that the proposed dual-wavelength injection P1 oscillation is an extension of laser dynamics theory, and the signal generation method is a promising solution for generating broadband frequency-modulated signals with good tunability.

https://doi.org/10.1364/OL.476499

Frequency-modulated (FM) microwave signals are widely used in radar systems [1]. To achieve a high range resolution, the FM signals transmitted by a radar should have a large spectral bandwidth. However, the generation of FM signals using electrical methods usually suffers from limited bandwidth. In recent years, microwave photonic approaches have been demonstrated to generate broadband microwave signals [2–4]. Among these methods, signal generation based on optically injected semiconductor lasers operating in the period-one (P1) oscillation state has attracted lots of attention because it has the advantages of a low cost, a simple structure, and good flexibility [5,6]. Up to now, P1 oscillation has been applied for generating tunable single-frequency signals [7], linear FM signals [8], and nonlinear FM signals [9]. In these systems, the light from a single-wavelength master laser (ML) is injected into a slave laser (SL), and FM signals are generated by fast tuning the injection strength [10]. This method can generate FM microwave signals with a large time–bandwidth product, but it requires at least an external electro-optical modulator and an electrical controlling signal generator to control the optical injection strength, resulting in a complicated structure with a high cost and potential stability problems.

In this Letter, we propose a new method for broadband FM microwave signal generation that uses dual-wavelength-injection P1 laser dynamics. To the best of our knowledge, this is the first time that dual-wavelength-injection-induced P1 laser dynamics has been used for microwave signal generation. In this method, the light from two MLs with different wavelengths is injected into an SL to excite P1 oscillation. The frequency beating between the two MLs causes frequency modulation of the P1 oscillation, based on which FM microwave signals can be generated. Because an external modulator and electrical controlling signal generator are not required, the proposed scheme has a compact structure and high stability. In addition, the frequency and bandwidth of the generated signals can be adjusted by properly controlling the injection parameters.

Figure 1 shows a schematic diagram of the proposed system. Two MLs (ML1 and ML2) generate two continuous-wave light beams at frequencies of f_1 and f_2, respectively. The frequency difference between ML1 and ML2 is $\Delta f = f_2 - f_1$. The two light beams are combined by an optical coupler (OC) and injected into an SL through an optical circulator (CIR). The free-running frequency of the SL is denoted by f_s. To maximize the injection efficiency, two polarization controllers (PC) are applied before the OC to align the polarizations of the MLs with that of the SL. By properly adjusting the optical injection strength and detuning frequencies between the MLs and the SL, P1 dynamics can be excited in the SL. Here, the injection strength is defined as the square root of the injection power of each ML divided by the power of the free-running SL, and the detuning frequency is defined as the frequency difference between each ML and SL ($f_{i1} = f_1 - f_s, f_{i2} = f_2 - f_s$). In traditional single-wavelength-injection P1 dynamics, the output signal from the SL contains a regenerated optical carrier and a redshifted cavity mode through the anti-guidance effect [11]. As a result, the P1 oscillation frequency is fixed and a single-frequency microwave signal is generated after optical-to-electrical conversion. For the proposed dual-wavelength injection P1 dynamics, the output signal from the SL contains two regenerated optical carriers at f_1 and f_2 and a redshifted cavity mode at f_s' ($f_s' < f_s$), as indicated by the spectrum at point *b* in Fig. 1. The frequency of

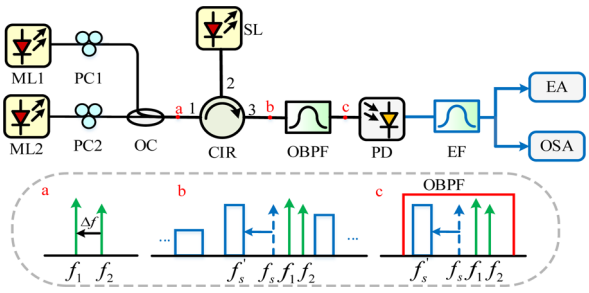

Fig. 1. Schematic diagram of the proposed dual-wavelength optically injected semiconductor laser system.

the redshifted cavity mode is sweeping because the frequency beating between the two regenerated optical carriers causes an amplitude modulation of the equivalent optical power injected into the SL. This leads to a variation of the P1 oscillation frequency. In this process, undesired frequency components are also generated due to nonlinear effects in the laser cavity, such as four-wave mixing (FWM) idlers. To remove these interferences, an optical bandpass filter (OBPF) is applied to select out the frequencies of f_1, f_2, and f_s', as shown by the spectrum at point c in Fig. 1.

In our system, to maximize the frequency beating efficiency between the two MLs, which is expected to enhance the frequency sweeping range of the redshifted cavity mode, the two MLs provide the same optical injection strength. In this case, the regenerated carriers at f_1 and f_2 have nearly the same amplitude. By properly setting the frequency difference Δf to let it be much smaller than the frequency of the desired FM signal, the low-frequency component at Δf after optical-to-electrical conversion at a photodetector (PD) can be removed using an electrical filter (EF), and the obtained signal can be expressed as

$$S(t) \propto \eta \cos(\pi \Delta f t) \cos[\pi(f_1 + f_2 - 2f_s')t]. \quad (1)$$

According to Eq. (1), an FM signal having an instantaneous frequency of $(f_1 + f_2 - 2f_s')/2$ is generated. Considering the fact that the P1 oscillation frequency is proportional to the optical injection power and the equivalent optical injection power generated by two MLs has a cosine profile, the frequency modulation in Eq. (1) also has a cosine form. The repetition rate of the generated FM signal equals Δf. In Eq. (1), η is a coefficient related to the amplitude fluctuation of the generated signal, which is caused by the fact that the dynamic competition between the regenerated optical carrier and redshifted optical sideband results in different amplitudes for different P1 oscillation frequencies. In practical applications, the amplitude fluctuation problem can be solved using power limiting techniques [12].

To get a deep understanding of the proposed dual-wavelength-injection P1 dynamics, numerical simulations are carried out in which the following nonlinear coupled equations are used to describe the laser dynamics:

$$\frac{da_r}{dt} = \frac{1}{2}\left[\frac{\gamma_n \gamma_c}{\gamma_s \tilde{J}}\tilde{n} - \gamma_p(a_r^2 + a_i^2 - 1)\right](a_r + b a_i) + \xi\gamma_c \cos(2\pi f_{i1} t) + \xi\gamma_c \cos(2\pi f_{i2} t) \quad (2)$$

$$\frac{da_i}{dt} = \frac{1}{2}\left[\frac{\gamma_n \gamma_c}{\gamma_s \tilde{J}}\tilde{n} - \gamma_p(a_r^2 + a_i^2 - 1)\right](-b a_r + a_i) - \xi\gamma_c \sin(2\pi f_{i1} t) - \xi\gamma_c \sin(2\pi f_{i2} t) \quad (3)$$

$$\frac{d\tilde{n}}{dt} = -[\gamma_s + \gamma_n(a_r^2 + a_i^2)]\tilde{n} - \gamma_s \tilde{J}(a_r^2 + a_i^2 - 1) + \frac{\gamma_s \gamma_p}{\gamma_c}\tilde{J}(a_r^2 + a_i^2)(a_r^2 + a_i^2 - 1). \quad (4)$$

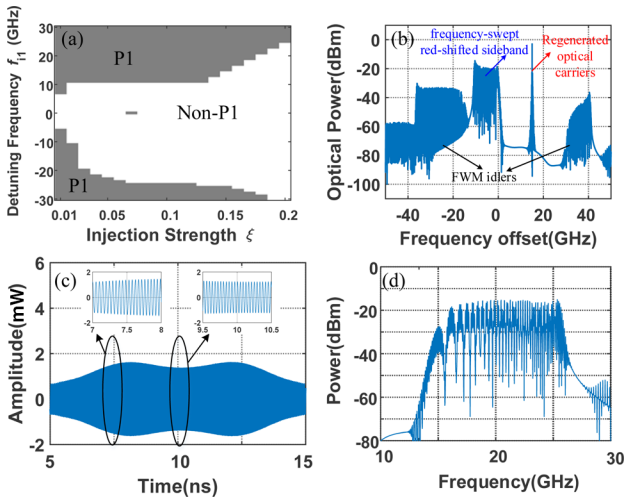

Fig. 2. Simulation results of (a) dynamic regions of the dual-wavelength optical injection, (b) optical spectrum of SL after optical injection, (c) temporal waveform, and (d) electrical spectrum of the generated FM microwave signal.

In these equations, a_r and a_i are the real and imaginary parts of the normalized total complex intracavity field amplitude of the slave laser, respectively. $\tilde{N}$ is the normalized carrier density. γ_n, γ_c, γ_s, γ_p, b, and $J^{\sim}$ denote the differential carrier relaxation rate, cavity decay rate, spontaneous carrier relaxation rate, nonlinear carrier relaxation rate, linewidth enhancement factor, and normalized injection current density, respectively. ξ is the injection strength of each ML. f_{i1} and f_{i2} are the detuning frequency of ML1 and ML2, respectively. In the coupled rate equation analysis, the device parameters are follows: $\gamma_n = 7.53 \times 10^9$ s^{-1}, $\gamma_c = 5.36 \times 10^{11}$ s^{-1}, $\gamma_s = 5.96 \times 10^9$ s^{-1}, $\gamma_p = 1.91 \times 10^{10}$ s^{-1}, $b = 3.2$, and $J^{\sim} = 1.222$ [13]. The relaxation oscillation frequency of the free-running laser is $f_r = (\gamma_c\ \gamma_n + \gamma_s\ \gamma_p)^{1/2}/2\pi = 10.25$ GHz. The fourth-order Runge–Kutta method is used to solve the coupled nonlinear equations, in which the temporal step and duration are 0.25 ps and 0.1 μs, respectively. The optical spectra are obtained from the Fourier transform of $a = a_r + ia_i$, and the sequence diagrams are obtained from $|a|^2$.

First of all, the nonlinear dynamic regions of the dual-wavelength optically injected semiconductor laser are numerically searched by varying the detuning frequencies (f_{i1} and f_{i2}) and the injection strength (ξ). The frequency difference between ML1 and ML2 is fixed to be 100 MHz. Figure 2(a) shows the result, in which the P1 regions are shown in dark gray and non-P1 regions are shown in white. Since the instantaneous injection power changes because of the frequency beating between the two MLs, the dynamic behavior also changes over time. In Fig. 2(a), the P1 regions refer to the areas in which only P1 dynamics are excited, even if the P1 oscillation frequency changes over time. However, for the non-P1 regions in Fig. 2(a), stable locking or chaos may appear in addition to P1 oscillation. In our system, only the P1 regions are considered for generating microwave signals with continuous frequency modulation. As an example, we show the simulation result for FM signal generation corresponding to a specific point in the P1 region. The injection parameters are $f_{i1} = 15$ GHz, $f_{i2} = 15.1$ GHz, and $\xi = 0.1$. Figure 2(b) shows the optical spectrum at the output of the SL after optical injection, which consists of two regenerated optical carriers, the frequency-swept redshifted optical sideband, as well

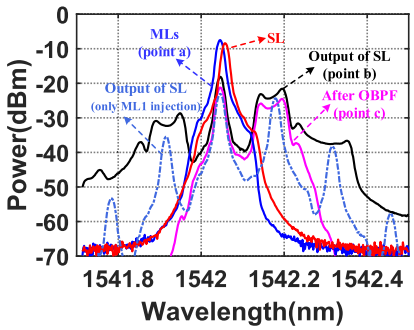

Fig. 3. Measured optical spectra of the injected MLs (blue line), the free-running SL (red line), and the SL output (black line), after the OBPF and dual-wavelength injection (magenta line), and the SL output after only ML1 injection (royal blue).

as the FWM idlers. Figure 2(c) shows the temporal waveform of the generated frequency-modulated signal. In Fig. 2(c), the amplitude of the generated signal fluctuates, which is related to the coefficient η. Figure 2(d) shows the corresponding electrical spectrum that covers the spectral range from 13.7 to 26 GHz.

To investigate the performance of the proposed method, an experiment is carried out based on the setup in Fig. 1. In the experiment, ML1 is a multi-channel tunable laser (CoBriteDX4) for which the wavelength can be tuned from 1527.6 nm to 1568.6 nm. ML2 is a tunable narrow-linewidth laser (TeraXion, PS-NLL-1550.12-040) for which the wavelength can be tuned from 1528.77 nm to 1563.86 nm. The SL is a distributed-feedback semiconductor laser (Actech LD15DM) with a free-running wavelength of 1542.058 nm. The SL is biased at 59.7 mA, about 10 times its threshold, and the free-running output power is 7.51 dBm. The optical spectra of the free-running SL and the combined two MLs are measured using an optical spectrum analyzer (OSA, Yokogawa AQ6370D) with a resolution of 0.02 nm, as shown in Fig. 3. Here, the light from each of the two MLs cannot be distinguished due to the limited resolution of the OSA. After optical injection, the optical spectrum of the signal from the SL is measured and shown in Fig. 3. As can be observed, the regenerated optical carriers, the redshifted, spectrally broadened sideband, and the FMW idlers are successfully generated. The optical spectrum obtained after removing the FWM idlers using an OBPF (Yenista XTM-50) is also shown in Fig. 3. The obtained optical signal is sent to a PD (u2t XPDV2120RA) with a bandwidth of 40 GHz to perform optical-to-electrical conversion. The generated FM microwave signal is observed by a real-time oscilloscope (Tektronix DSA72004B) working with a sampling rate of 50 GSa/s. As a comparison, the optical spectrum of P1 oscillation under single-wavelength (ML1) injection is also shown in Fig. 3. In this case, single-frequency P1 oscillation is excited, in which the spectrum mainly contains a regenerated optical carrier and a narrow redshifted sideband.

To show the FM signal generation capability, the wavelengths of ML1 and ML2 are set to 1542.045 nm and 1542.0443 nm, respectively. The detuning frequencies of the two MLs are $f_{i1} = 1.64$ GHz and $f_{i2} = 1.728$ GHz, respectively, and the frequency difference $\Delta f = 88$ MHz. The injection strength of each ML is $\xi = 1.33$. The waveform of the generated FM signal is shown in Fig. 4(a). As can be observed, an amplitude fluctuation appears in the generated waveform, which is similar to the simulation result in Fig. 2(a). Figure 4(b) shows

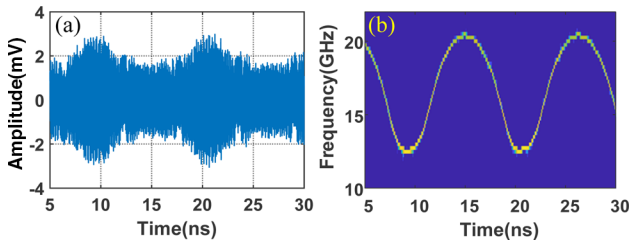

Fig. 4. (a) Measured waveform and (b) recovered instantaneous frequency of the experimentally generated FM microwave signal.

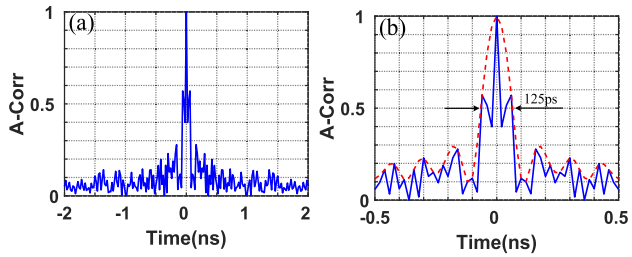

Fig. 5. (a) Autocorrelation result for the generated FM signal and (b) enlarged view of the autocorrelation peak.

the instantaneous frequency of the generated signal, which is obtained by performing short-time Fourier transformation. The recovered instantaneous frequency has a cosine function profile, and the generated signal has a bandwidth of 8 GHz (12.25–20.25 GHz). The temporal period of the generated signal is found to be 11.3 ns, indicating that the repetition rate of the generated signal equals the frequency difference Δf. To test the pulse compression capability, the autocorrelation of the FM signal is calculated, as shown in Fig. 5(a), in which a narrow peak is clearly observed. In the zoomed-in view shown in Fig. 5(b), the full width at half-maximum of the autocorrelation peak is 125 ps. The corresponding radar range resolution is 1.875 cm, which agrees well with the theoretical value.

For the proposed system, the frequency and bandwidth of the generated FM signals are determined by the injection strength and detuning frequencies of the two MLs. Thus, they can be easily adjusted by properly setting the injection strength and detuning frequencies. To investigate the influence of injection strength on the generated signal frequency and bandwidth, the detuning frequencies of the two MLs are fixed to be 1.64 GHz and 1.918 GHz, respectively. The corresponding frequency difference Δf is 278 MHz. When the injection strength of each ML is increased from 0.53 to 1.33, the frequency ranges of the generated FM signals are measured and shown in Fig. 6(a). As can be seen, as the injection strength increases, both the bandwidth and the central frequency of the generated FM signal are increased. This is caused by the fact that a high injection strength of each ML leads to a large variation of the frequency beating amplitude, which induces a large variation of the P1 oscillation frequency. Figures 6(b)–6(d) show the instantaneous frequencies of the generated signals when the injection strength is 0.53, 0.84, and 1.33, respectively. The signal bandwidths are 2.25 GHz (10.75–13 GHz), 5.25 GHz (11.25–16.5 GHz), and 8 GHz (12.25–20.25 GHz), respectively.

Next, the influence of the detuning frequencies on the generated signal frequency and bandwidth is investigated. To this end, the injection strength of each ML is fixed to be 0.943,

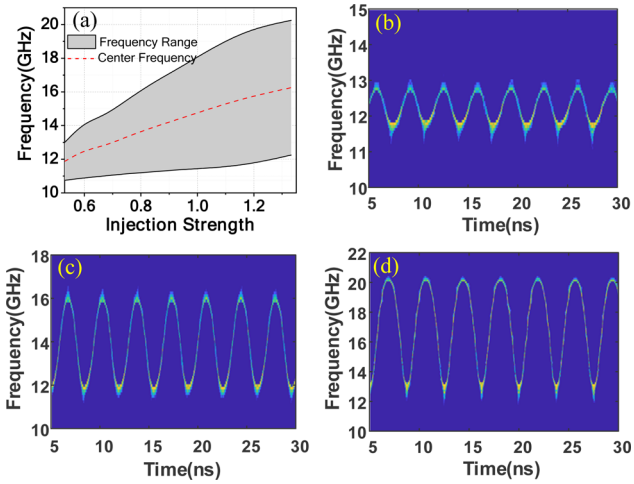

Fig. 6. (a) Frequency range of the generated signal under different injection strengths; (b), (c), and (d) recovered instantaneous frequency when the injection strength is 0.53, 0.84, and 1.33, respectively.

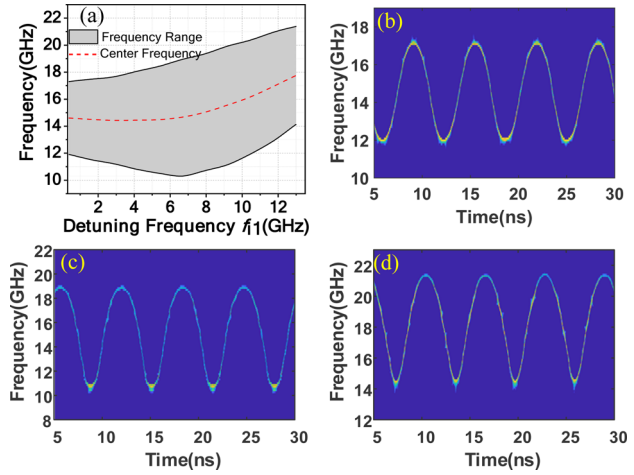

Fig. 7. (a) Frequency range of the generated signal under different detuning frequencies; (b), (c), and (d) recovered instantaneous frequency when the detuning frequency is 0.38 GHz, 6.69 GHz, and 12.995 GHz, respectively.

and the detuning frequency f_{i1} is adjusted from 0.38 GHz to 12.995 GHz. The detuning frequency f_{i2} is adjusted simultaneously in a manner that the frequency difference between the two MLs is kept to 160 MHz. Figure 7(a) shows the measured frequency ranges of the generated FM signals as detuning frequency f_{i1} changes. It is obvious that, when detuning frequency f_{i1} is increased from 0.38 GHz to around 6.69 GHz, the bandwidth of the generated FM signal is increased while the center frequency is slightly reduced. Figures 7(b) and 7(c) show the recovered instantaneous frequency of the generated signals when detuning frequency f_{i1} is 0.38 GHz and 6.69 GHz, respectively. The corresponding bandwidth is 5.4 GHz (11.9–17.3 GHz) and 8.7 GHz (10.3–19 GHz), respectively. As the detuning frequency f_{i1} is further increased to 12.995 GHz, the generated signal bandwidth is reduced while the center frequency is increased. Figure 7(d) shows the instantaneous frequency of the generated signal when detuning frequency f_{i1} is 12.995 GHz, where the bandwidth is reduced to 7.25 GHz (14.13–21.38 GHz). The reason for the frequency variation in Fig. 7(a) is as follows. When the detuning frequency is small, the P1 oscillation is also affected by the injection pulling effect [14], which pulls the redshifted optical sideband toward the injected optical frequency and hence decreases the bandwidth of the generated FM signal. For a large detuning frequency, the increase in detuning frequency tends to elevate the P1 oscillation frequency and lower the frequency modulation efficiency of P1 oscillation [15], which leads to a reduced bandwidth of the generated signal.

The above investigations soundly verify the feasibility of the proposed FM signal generation method, although there are several issues that need to be clarified. First, the spectral range of generated signals in the experiment was limited by the devices used. If devices having a larger operation bandwidth are used, the frequency and bandwidth of the generated FM signals can be further expanded. Second, the proposed concept can be extended to optical injection with more than two wavelengths. By controlling the equivalent injection power, FM signals with other formats such as sawtooth and triangular profiles can be generated. Third, to improve the spectral stability and suppress the phase noise, optical or optoelectronic feedback mechanisms can be incorporated into the proposed system.

Funding. National Key Research and Development Program of China (2021YFB2800803); National Natural Science Foundation of China (61871214); Natural Science Foundation of Jiangsu Province (BK20221479); Fund of Prospective Layout of Scientific Research for NUAA.

Disclosures. The authors declare no conflicts of interest.

Data availability. Data underlying the results presented in this Letter are not publicly available at this time but may be obtained from the authors upon reasonable request.

REFERENCES

1. A. Meta, P. Hoogeboom, and L. P. Ligthart, IEEE Trans. Geosci. Remote Sensing **45**, 3519 (2007).
2. J. Yao, J. Lightwave Technol. **27**, 314 (2009).
3. F. Zhang, Q. Guo, and S. Pan, Sci. Rep. **7**, 13848 (2017).
4. F. Zhang, Q. Guo, Z. Wang, P. Zhou, G. Zhang, J. Sun, and S. Pan, Opt. Express **25**, 16274 (2017).
5. S. K. Hwang, J. M. Liu, and J. K. White, IEEE J. Quantum Electron. **10**, 974 (2004).
6. C. Chu, S. L. Lin, S. C. Chan, and S. K. Hwang, IEEE J. Quantum Electron. **48**, 1389 (2012).
7. J. S. Suelzer, T. B. Simpson, P. Devgan, and N. G. Usechak, Opt. Lett. **42**, 3181 (2017).
8. G. Sun, F. Zhang, and S. Pan, Opt. Lett. **46**, 5659 (2021).
9. J. Zhuang, X. Li, S. Li, and S. C. Chan, Opt. Lett. **41**, 5764 (2016).
10. P. Zhou, F. Zhang, Q. Guo, M. Li, and S. Pan, IEEE J. Quantum Electron. **23**, 1 (2017).
11. S. C. Chan, IEEE J. Quantum Electron. **46**, 421 (2010).
12. J. W. Shi, F. M. Kuo, N. W. Chen, S. Y. Set, C. B. Huang, and J. E. Bowers, IEEE Photonics J. **4**, 215 (2012).
13. S. K. Hwang, J. Liu, and J. K. White, IEEE Photonics Technol. Lett. **16**, 972 (2004).
14. T. Simpson, J. Liu, M. AlMulla, N. Usechak, and V. Kovanis, Phys. Rev. Lett. **112**, 023901 (2014).
15. S. C. Chan, S. K. Hwang, and J. Liu, Opt. Express **15**, 14921 (2007).